



LAWRENCE
LIVERMORE
NATIONAL
LABORATORY

Performance of indirectly-driven capsule implosions on NIF using adiabat-shaping

H. F. Robey

December 1, 2015

APS DPP 2015
Savannah, GA, United States
November 16, 2015 through November 20, 2015

Disclaimer

This document was prepared as an account of work sponsored by an agency of the United States government. Neither the United States government nor Lawrence Livermore National Security, LLC, nor any of their employees makes any warranty, expressed or implied, or assumes any legal liability or responsibility for the accuracy, completeness, or usefulness of any information, apparatus, product, or process disclosed, or represents that its use would not infringe privately owned rights. Reference herein to any specific commercial product, process, or service by trade name, trademark, manufacturer, or otherwise does not necessarily constitute or imply its endorsement, recommendation, or favoring by the United States government or Lawrence Livermore National Security, LLC. The views and opinions of authors expressed herein do not necessarily state or reflect those of the United States government or Lawrence Livermore National Security, LLC, and shall not be used for advertising or product endorsement purposes.

Performance of indirectly driven capsule implosions on NIF using adiabat-shaping

H. F. Robey¹, V. A. Smalyuk¹, J. L. Milovich¹, T. Döppner¹, D. T. Casey¹, K. L. Baker¹,
J. L. Peterson¹, B. Bachmann¹, L. F. Berzak Hopkins¹, E. Bond¹, J. A. Caggiano¹, D. A.
Callahan¹, P. M. Celliers¹, C. Cerjan¹, D. S. Clark¹, S. N. Dixit¹, M. J. Edwards¹, N. Gharibyan¹,
S. W. Haan¹, B. A. Hammel¹, A. V. Hamza¹, R. Hatarik¹, O. A. Hurricane¹, K. S. Jancaitis¹,
O. S. Jones¹, G. D. Kerbel¹, J. J. Kroll¹, K. N. Lafortune¹, O. L. Landen¹, T. Ma¹, M. M.
Marinak¹, B. J. MacGowan¹, A. G. MacPhee¹, A. Pak¹, M. Patel¹, P. K. Patel¹, L. J. Perkins¹,
D. B. Sayre¹, S. M. Sepke¹, B. K. Spears¹, R. Tommasini¹, C. R. Weber¹, C. C. Widmayer¹,
C. Yeaman¹, E. Giraldez², D. Hoover², A. Nikroo², M. Hohenberger³, and M. Gatu Johnson⁴

1) Lawrence Livermore National Laboratory, USA 94551

2) General Atomics, San Diego, CA 92186

3) Laboratory for Laser Energetics, Rochester, NY 14623

*4) Plasma Science and Fusion Center, Massachusetts Institute of Technology,
Cambridge, MA 02139*

ABSTRACT

A series of indirectly driven capsule implosions has been performed on the National Ignition Facility to assess the relative contributions of ablation-front instability growth vs. fuel compression on implosion performance. Laser pulse shapes for both low and high-foot pulses were modified to vary ablation-front growth & fuel adiabat, separately and controllably. Three principal conclusions are drawn from this study: 1) It is shown that reducing ablation-front instability growth in low-foot implosions results in a substantial (3-10X) increase in neutron yield with no loss of fuel compression. 2.) It is shown that reducing the fuel adiabat in high-foot implosions results in a significant (36%) increase in fuel compression together with a small (10%) increase in neutron yield. 3.) Increased electron preheat at higher laser power in high-foot implosions, however, appears to offset the gain in compression achieved by adiabat-shaping at lower power. These results taken collectively bridge the space between the higher compression low-foot results and the higher yield high-foot results.

I. INTRODUCTION

Inertial confinement fusion (ICF) implosion experiments are being conducted on the National Ignition Facility (NIF) [1] with a goal of compressing a spherically layered cryogenic shell of deuterium tritium (DT) fuel [2] to a sufficient areal density (ρR) to inertially confine the hot fuel for a sufficient duration to sustain a self-propagating burn wave, which is required for the DT fusion power gain to exceed unity. Most experiments on the NIF employ the indirect-drive technique [3], where the energy of a precisely tailored sequence of laser pulses is converted into a thermal x-ray bath inside a high-Z (typically Au or depleted uranium, DU) enclosure called a hohlraum. This x-ray radiation ablates the outer surface of a low-Z (typically polystyrene (CH) [4], high-density carbon [5], or Be [6]) spherical shell, which surrounds the cryogenic layer of DT fuel, compressing the fuel to create the high temperature plasma conditions required to initiate DT fusion reactions in the central hot spot core.

A number of factors are critical to the success of these implosions. Principal among these are the following: 1.) minimizing the growth of perturbations on the ablation surface, which are unstable to both the Rayleigh-Taylor [7, 8] and Richtmyer-Meshkov instabilities [9-15], 2) maintaining the DT fuel layer on a low adiabat (ratio of the mass-averaged fuel pressure to the Fermi degenerate pressure [4, 16]) to maximize compressibility, and 3) controlling low-mode shape distortions of the compressed fuel layer arising from intrinsic asymmetries in the hohlraum radiation drive [17, 18]. The first two of these factors, ablation-front instability and fuel compressibility, will be the focus of this study. Also of importance, as will be discussed in Section V, is the role of high-energy electron preheat, which can adversely affect the fuel adiabat as one increases the laser power to drive higher velocity implosions.

The trade-off between stability and compression is illustrated in Figure 1, which shows a plot of measured neutron yield vs. neutron down-scattered ratio (DSR, the ratio of neutrons with down-scattered energies from 10-12 MeV over the un-scattered fraction with energies from 13-15 MeV) for all NIF layered implosions to date. Three separate regions of this parameter space are highlighted. The blue points are “low-foot” (LF) implosions conducted during the National Ignition Campaign [19]. These implosions exhibited relatively higher compression (fuel areal density ρR in $\text{g}/\text{cm}^2 \sim 0.2 \cdot \text{DSR}$ in %), but were found to have a significant problem with

ablation-front instability leading to the mixing of ablator material into the DT fuel [20, 21]. The green points, by contrast, are “high-foot” (HF) implosions [22-24], which were conducted at a higher fuel adiabat and reduced convergence to minimize performance degradations due to instability growth. These implosions were very successful in achieving higher yields, but this was done at the expense of a reduced fuel areal density ($\rho R < 0.8$, $DSR < 4.0$). In the present study, we ask the following 2 questions: First, can the high compression of low-foot implosions be maintained while reducing ablation-front instability, and does this increase yield? Second, can the high yield of high-foot implosions be maintained, while moving to higher compression? The three magenta points, which are the focus of the present paper, are the result of applying adiabat-shaping to both low and high-foot implosions and, as will be shown, provide an affirmative answer to both of these questions.

Adiabat-shaping, a technique wherein the ablator is deliberately put on a high adiabat to promote increased ablation-front stability and the fuel is maintained at a low adiabat to maintain good fuel compressibility has been extensively investigated in previous studies. The concept was first studied in [25-27] and subsequently explored in direct-drive implosion experiments on the OMEGA Laser Facility in [28-31].

Most previous studies employed adiabat-shaping in directly-driven implosions. Ref. [32] was the first to demonstrate that the temporal response of a hohlraum was sufficiently fast to allow adiabat-shaping to be extended to indirectly-driven implosions as well. An additional difference from previous studies is that in the present work adiabat-shaping is used to affect the earlier RM instability phase as opposed to the later-time RT phase. References [33, 34] extend the work of previous studies on the ablative RM instability [11-15] to show that in indirectly-driven implosions, the phase of ablative RM oscillations can be deliberately tuned, so that minimal RM growth is achieved at mode numbers where the subsequent RT growth is the largest. This results in reduced overall instability growth as demonstrated experimentally in [35-39]. A survey of the design space was performed in [34], where it was shown that separate portions of the laser pulse could be adjusted to controllably and independently alter either the ablation-front stability or the fuel compression. Specifically, it was demonstrated that increasing the initial laser picket improves ablation-front stability at relatively constant compression, while decreasing the low-power laser trough improves compression at similar stability.

This paper is organized as follows. In Sections II and III, the fuel adiabat and ablation-front stability, respectively, are quantified by experiment and are compared with previous results. In Section IV, the performance of the three adiabat-shaped layered DT implosions of Figure 1 is described. Section V discusses both experimental observations and numerical simulations of the effect of electron preheat on implosion performance. Finally, Section VI summarizes the results and discusses future directions.

II. QUANTIFYING THE FUEL ADIABAT AND ABLATION-FRONT STABILITY

12 shots were performed in this campaign to assess the performance of two new adiabat-shaped (AS) laser pulses. Table I summarizes the shot type and purpose. For adiabat-shaped versions of both a low and a high-foot laser pulse, keyhole shots [40, 41] were performed to quantify the fuel adiabat, Hydro-Growth Radiography (HGR) shots [35, 36] quantified the ablation-front instability growth, and 2DConA shots [42] were used to assess the implosion shape and velocity. For both AS LF and AS HF pulses, layered DT shots were performed at relatively low peak laser power (325-340 TW). For the AS HF pulse, an additional layered DT shot was performed at higher power (390 TW). The shot numbers are listed in Table I.

TABLE 1. Summary of shots performed in the adiabat-shaping campaign

Shot type:	Quantifies:	Adiabat-shaped Low-foot (LF)	Adiabat-shaped High-foot (HF)
Keyhole	Adiabat	N140611 N140919	N140718 N150203
HGR	Ablation-front growth	N140629 N150118	N140818
2DConA	Shape, velocity	N141014	N141028
Layered DT @ reduced power	Yield, DSR, etc.	N141123	N150115
Layered DT @ increased power	Yield, DSR, etc.	-	N150416

As was shown in Clark [34], very small changes to the early time portion (the “foot”) of the laser pulse can have a significant impact. Small changes to the picket power were found to strongly affect ablation-front stability, while small changes to the trough power were shown to affect the fuel adiabat. The sensitivity of the shock timing to these small changes was extensively discussed in Baker [43]. Figure 2(a) shows the specific changes that were made to both the low and high-foot laser pulses in this study. The pulses shown in Figure 2(a) are similar to those discussed in [43], with the addition of AS HF #2 (orange, shot N150203), which was performed after publication of reference [43], and which plays a key role in discussing the performance of DT layered implosions in the Section IV. The standard low-foot (black) and high-foot (red) pulses are shown with dashed lines. The 4-step LF pulse is 50% longer in duration (21 ns) than the 3-step HF pulse (14 ns), and as the name LF implies, it has significantly lower energy in both the initial picket (LF: 15 kJ, HF: 38 kJ) and the trough (LF: 13 kJ, HF: 25 kJ). The adiabat-shaped (AS) versions of the low-foot (blue) and high-foot (green, orange) pulses are shown with solid lines. The two AS HF pulses (AS HF #1 green, AS HF #2 orange) are nominally identical with the exception that the 2nd and 3rd pulses for AS HF #2 were advanced in time by 700 ps. This was done to achieve proper shock merger timing for the 20 μm thinner ablator used in AS HF #2.

The picket energy of the AS LF pulse was increased from 15 to 23 kJ by extending the duration of the picket by ~ 400 ps. Note that this is still low compared to the standard high-foot pulse, which has picket energy of 38 kJ. This will be of importance in evaluating the relative stability in Section III. In contrast, no change was made to the picket of the AS HF pulses. The trough power of the AS HF pulses was decreased from 4.0 to 1.0 TW. The timing of subsequent higher-power portions of all AS pulses was advanced to achieve proper shock merger timing. This results in all three AS pulses being of similar duration (~ 16 -17 ns), a value that is intermediate between the standard LF and HF pulses. Note that the total changes in pulse energy that have been made are very small. For all AS pulses, the total laser pulse energy is changed by less than 0.5% from the standard LF and HF companion pulses. These minimal changes, however, will be shown to have very significant effects on both the ablation-front stability and the fuel compression.

For all keyhole shots listed in Table I, the VISAR (Velocity Interferometer System for Any Reflector) diagnostic [44, 45] was used to diagnose the velocity history and merger timing of the

resulting shocks in both the ablator and the surrogate D2 fuel. Figure 2(b) shows the VISAR-measured velocity histories of the leading shock front for each of the pulses of Figure 2(a). The entire shock velocity history for all AS pulses falls between those of the standard HF and LF. The velocity of the 1st shock is important, as it adds most of the entropy ($\Delta s \sim \Delta Q_{\text{fuel}}/T_{\text{fuel}}$) to the fuel, since the 1st shock heating (ΔQ_{fuel}) occurs while the fuel temperature T_{fuel} is still quite low. The first shock velocity for the AS LF (blue, 19.0 $\mu\text{m/ns}$) is very comparable to that of the standard LF (black, 18.5 $\mu\text{m/ns}$) as intended, since no change was made to the trough of the laser pulse, which controls the 1st shock velocity [41]. The average first shock velocity for the two AS HF pulses are a little higher than the two LF pulses at 22.2 (green) and 20.45 $\mu\text{m/ns}$ (orange) for AS HF #1 and #2, respectively. Both are substantially lower than the standard HF pulse, though, which has a first shock velocity of 29.7 $\mu\text{m/ns}$ (red).

One-dimensional simulations using the radiation-hydrodynamics code HYDRA [46], tuned to precisely match the VISAR-measured velocity histories of Figure 2(b), can be used to extract the radial pressure profile through the ablator and fuel regions. This is shown in Figure 3(a) where the pressure behind the leading shock is plotted as a function of radius. This Figure gives a good visual signature of “adiabat-shaping” in these pulses. For the HF pulse (red, dashed), pressure is higher throughout both ablator and fuel. This is good for ablation-front stability, but bad for fuel compression. For the low-foot pulse, the reverse is true. Pressure is low throughout. This is bad for ablation-front stability, but good for fuel compression. The adiabat-shaped pulses are designed to achieve the best of both worlds, namely both good stability and good fuel compression. All three adiabat-shaped pulses show a pronounced decay from a high pressure at the ablation front (good for stability) to a low value in the fuel (good for compression). Comparing the HF and LF pulses, the LF pulse still has slightly lower ablation-front stability but slightly better compression. From the tuned simulations, the temporal history of the fuel adiabat can be quantified. The procedure is the following: The simulations, tuned to the VISAR shock velocity data obtained in liquid D2-filled keyholes, are re-tuned to obtain ideal shock merger timing appropriate for a layered DT implosion. Simulations are then re-run in a layered DT configuration, and the mass-averaged fuel adiabat is extracted. The temporal history of the simulated adiabat is plotted in Figure 3(b). The various steps seen in these adiabat time histories correspond to the entropy added during the traversal of the sequential shocks. The circle symbols indicate the value of the fuel adiabat at the time of peak fuel velocity. The adiabat

values are 2.3 (HF, red), 2.1 (AS HF #1, green), 2.0 (AS HF #2, orange), 1.6 (AS LF), and 1.5 (LF, black). Note that a significant difference remains in the adiabats of the LF and HF cases. This is simply due to the difference in the number of driving pulses (3 for all HF-based pulses and 4 for all LF-based pulses), and therefore the number of shocks and corresponding pressure jumps seen in the fuel [see 47, Figure 4.5]. Note also that even though the requested foot power of both AS HF pulses was the same, the delivered power histories were slightly different with AS HF #2 (N150203) delivering 6% lower power in the picket and 8% lower power in the trough as compared to that delivered in AS HF #1 (N140718). This is the reason for the observed slightly lower shock velocities (orange vs. green) in Figure 2(b) as well as the slightly lower adiabat of Figure 3(b). This difference would lead one to expect slightly higher compression in the corresponding layered DT implosions, which will be discussed in Section IV.

III. QUANTIFYING THE ABLATION-FRONT STABILITY

Having discussed the effect of these small changes to the foot of the laser pulse on the fuel adiabat, we now turn our attention to the corresponding effect of these same modifications on the ablation-front stability. Much of this has been previously reported in refs. [33-39], though a full comparison of all shots performed to date has not yet been reported. This Section therefore serves as a summary of that work, comparing experimental results and predictions for all standard and AS pulses tested in this campaign. Figure 4(a) shows simulated ablation-front growth factor dispersion curves for the LF, HF, AS LF and AS HF #1 pulses. The growth factor is defined as the perturbation amplitude at the time of peak fuel velocity divided by its amplitude at $t = 0$. (Simulations are not included in Figure 4(a) for the AS HF #2 pulse of Figure 2(a), which used a thinner ablator, as those experiments have not yet been performed. The results are expected to be very similar to those of AS HF #1, however.) As seen in Figure 4(a), the standard HF pulse (red, dashed) shows 4X less ablation-front growth than the LF (black, dashed) pulse. This comparison is extensively discussed in Casey [37]. Adiabatic-shaping of the LF pulse (blue) by increasing the picket energy is predicted to reduce growth substantially, though with increased growth in the phase-inverted modes (80-200). Note that the mode number of the onset of phase reversal for the AS LF pulse is predicted to be at \sim mode 80, similar to that seen for the

HF pulse. Adiabatic-shaping of the HF pulse (green) is predicted to give similar, though slightly reduced, growth to that seen in the standard HF pulse (red).

Figure 4(b) shows a schematic of the experimental geometry that is used on NIF in the Hydro-Growth Radiography (HGR) target platform. This geometry and the initial experiments are described in detail in refs. [35, 36]. A standard NIF hohlraum and capsule are used. A Au diagnostic cone, similar to that used in keyhole experiments [40], is used to provide a diagnostic line-of-sight for the 4.3 keV backlighter x rays, which are produced by interaction of two quads incident on a Vanadium foil located outside the hohlraum. The capsule is precisely machined with sinusoidal perturbations of very small initial amplitude on the outer surface within the field-of-view of the diagnostic x-ray framing camera. A comparison of the resulting optical depth modulations in the x-ray images at a capsule radius of $\sim 650 \mu\text{m}$ (convergence of $\sim 2X$) is shown in Figure 4(c) for all four pulses. The agreement with the predicted growth of Figure 4(a) is very good. Growth in the HF implosions is measured to be $\sim 4X$ less than that of the LF, and both AS pulses show similar growth to that of the HF pulse. Note that phase inversion of the adiabatic-shaped LF pulse is also observed as predicted around mode 80.

As indicated in Table I, 2DConA shots were also performed for each of the AS pulses. 2DConA shots use a target geometry similar to that shown in Figure 4(b), but without the Au diagnostic cone, to obtain images of the shape of imploded surrogate capsules at a radius of $\sim 200 \mu\text{m}$. An important observation from these images was that in the more unstable LF implosions performed during the NIC, a very clear pair of azimuthal rings of decreased areal density ρR were seen at polar angles of $\sim 45^\circ$ from the capsule poles. These features have been attributed to the unstable growth of an initial perturbation caused by the thin capsule support tent, which departs from the capsule near the observed feature location. This feature is extensively discussed in refs. [48-50]. In reference [50], it was shown that this tent-induced feature is much more pronounced in LF implosions than in HF implosions. Similar results were recently reported [51] for adiabatic-shaped LF 2DConA shot N141014, where again the tent feature was not visible in the radiographic image. This observation gives an additional visual confirmation that ablation-front growth is reduced in adiabatic-shaped pulses.

IV. PERFORMANCE OF ADIABAT-SHAPED DT LAYERED IMPLOSIONS

In this Section, the performance of the three adiabat-shaped implosions of Figure 1 is discussed. We begin with a discussion of the AS LF pulse (blue) of Figure 2(a). To summarize earlier observations, this pulse showed a very similar adiabat in Figure 3(b) but significantly improved stability in comparison to the standard LF pulse in Figure 4(c). Figure 5(a) shows the parameter space of neutron yield vs. DSR for all NIF shots. Shot N141123 (highlighted in magenta) was an AS LF shot with a total laser energy of 1.6 MJ and a peak laser power of 336 TW. It is compared in Figure 5(a) with 5 shots from the NIC database that had very similar laser power and energy. Complete experimental details of this shot are given in Casey [52], and comparison with numerical simulation is discussed in Milovich [51]. As pointed out in those publications, this shot exhibited a 3-10X increase in neutron yield with no loss of compression as compared to its companion shots. The degree of alpha heating as indicated by the dashed contours in Figure 5(a) was 1.5X, a value comparable to a similar power (325 TW) and energy (1.6 MJ) HF shot N150610 (circled in green). These results very strongly indicate that ablation-front growth was indeed a major factor in degrading the yield of NIC LF implosions.

This shot raises the question of how much further performance can be improved by adiabat-shaping. Figure 5(b) shows the very strong sensitivity of the ablation-front growth to the picket laser energy. The request picket energy for shot N141123 was 23 kJ, but the as-delivered shot energy was 5.5% lower at 21.8 kJ. This very small reduction in the delivered picket energy is predicted to increase peak ablation-front growth near mode 50 from 380 to 600, a 60% increase. On the other hand, simulations show that further increasing the picket energy to 30 kJ improves stability by an additional factor of two over that observed on shot N141123, with no further increase in fuel adiabat. The HF pulse, by comparison, is even more stable with a picket energy of 38 kJ, though at this picket energy the adiabat begins to increase, as the hohlraum can no longer cool quickly enough to keep the fuel entropy at a minimum.

Also shown in Figure 5(b) is the estimated growth of the tent feature, which has a dominant localized mode number of ~ 30 . The growth at this mode number was decreased by 31% on N141123 (black) relative to the standard LF pulse (red). Growth of this localized feature can also be reduced by an additional factor of two by a further increase in picket energy (green). It seems likely that increasing the picket energy of the AS LF to 30 kJ would further increase the yield to a value comparable to HF shot N150610, though this experiment is yet to be performed.

We now turn to the performance of the two AS HF pulses shown in Figure 2(a). To review the previous observations, these showed a moderately reduced adiabat in Figure 3(b) and similar stability to the standard HF in Figure 4(c). Figure 6(a) plots the laser power histories for AS HF #1 (N150115, magenta, dashed) and AS HF #2 (N150416, magenta, solid) together with their companion HF pulses N150610 (green, dashed) and N140520 (green, solid). For both AS pulses, the trough power is lower, and the subsequent pulses are delayed slightly to achieve good shock merger timing. Beginning with the lower power pulses, AS HF #1 (N150115) showed a significant increase in DSR (36%) and a modest (10%) increase in yield over similar power high-foot companion shot N150610. This is a clear consequence of the decreased adiabat of Figure 3(b). X-ray hot-spot size also decreased by $\sim 23\%$ from 35.5 to 29.0 μm , suggesting that increased convergence is possible without impacting the performance of high-foot implosions. Further details of the performance of shot N150115 are presented in [53].

Increasing laser power in the adiabat-shaped pulse, however, resulted in a much more modest increase in DSR. In shot N150416, a 20 μm thinner capsule was used, peak laser power was increased from 328 to 388 TW, and total laser energy was increased from 1.58 to 1.74 MJ. The foot of the pulse remained the same, however, and the adiabat was expected from Figure 3(b) to decrease slightly from the lower power AS HF shot N150115. This should correspond to increased ρR and a higher measured DSR. As Figure 6(b) shows, however, the DSR increased over companion high-foot shots N140520, N150121, and N150409 by only 14%, as opposed to the 36% increase seen at lower power. The DSR on shot N150416 (4.65%) actually decreased relative to that of shot N15015 (5.04%), contrary to expectations from the measured adiabats of Figure 3(b). Total neutron yield (including the down-scattered component) was $8.41\text{e}15$, very comparable to similar high-foot shots N140520 ($8.98\text{e}15$), N150121 ($7.33\text{e}15$), and N150409 ($8.07\text{e}15$).

The comparison of the two AS HF shots clearly shows that compression is being compromised as the laser power is increased. This is supported by two additional experimental observations shown in Figure 7. Figure 7(a) shows that the decrease in DSR with laser power is consistent with radiochemistry measurements of Au isotope ratios. As was shown in Shaughnessy [54], the ratio of isotope concentrations produced in Au hohlraums due to interactions with primary and down-scattered neutrons is proportional to fuel compression, DSR. Down-scattered neutrons do not contribute to the production of ^{196}Au , an (n,2n) reaction, which

has a threshold response, but do contribute to the production of ^{198}Au , an (n,γ) reaction. As is seen in Figure 7(a), as the DSR decreases from shot N141123 to N150115 to N150416, the Au isotope ratio decreases correspondingly. Even though the laser power and energy are increased from N150115 to N150416, the compression as measured by both diagnostics (DSR and Au isotope ratios) decreases. This is counterintuitive, and implies that some additional physics is playing a role. The measured x-ray hot-spot size shown in Figure 7(b) further confirms this observation. In Figure 7(b), it is seen that the AS hot-spot radii are essentially the same at lower and higher laser power, indicating that the capsule compression did not respond to the increased laser drive. In the next Section, a plausible explanation for these observations is discussed.

V. IMPACT OF ELECTRON PREHEAT WITH INCREASING LASER POWER

A possible explanation for the lack of increased compression is that electron preheat may be having more of an impact as laser power is increased. Figure 8(a) shows images from the eHXI (equatorial Hard X-ray Imager) diagnostic [55], which measures the spatial distribution of hard x-ray emission associated with supra-thermal electrons in NIF hohlraums. In Figure 8(a), images are shown (same color scale) for the two AS HF implosions, N150115 at lower peak power and N150416 at higher power. A clear increase in hard x-ray emission is seen with increasing power. Figure 8(b) shows vertical line-outs taken through the center of these images showing that as laser power is increased from 328 to 388 TW (N150115 to N150416), the hard x-ray signal measured by eHXI nearly doubles. This increase in electron preheat will affect the fuel adiabat, possibly counteracting the gains achieved by adiabat-shaping as shown in Figure 3(b).

To evaluate this possibility, numerical simulations have been performed using HYDRA to assess the impact of supra-thermal electron preheat on fuel compression. Electron preheat arising from both Stimulated Raman Scattering (SRS, 18 keV) and Two-Plasmon Decay (TPD, ~ 100 keV) sources was added to integrated hohlraum simulations using a supra-thermal model in HYDRA. This model incorporates a supra-thermal electron flux using a nonlocal electron transport model, which is an extension to three-dimensions of the model of Shurtz, Nikolai, and Busquet [56]. The HYDRA supra-thermal model has been augmented to include energy cascading, where as electrons slow down, their scattering cross-section increases and the

stopping power increases. Contributions to the stopping power due to scattering from bound electrons and bare ions are included as well [57, 58].

The time dependence of the supra-thermal preheat is taken from NIF backscatter & FFLEX measurements for the 18 and 100 keV components, respectively. Source energies for the 18 and 100 keV components are estimated in these simulations as one half of the SRS backscattered energy and the FFLEX-measured 100 keV energy, respectively. For shot N150115, the measured SRS backscattered energy was 166 kJ. The 18 keV preheat energy is therefore taken to be 83 kJ, and the TPD preheat energy measured from FFLEX is 2.3 kJ. For N150416, the SRS backscatter was 212 kJ, and the preheat source energies are 106 and 3.6 kJ, respectively. A plot of the relative power and timing of these sources is shown in Figure 9(a) with the lower power shot N150115 in blue and the higher power shot N150416 in red. The measured laser power histories are shown with dashed lines, and the relative timing of the SRS sources (early) and TPD sources (late) are as indicated. The power of the TPD source has been multiplied by 100x in Figure 9(a) to see it on the same scale as the laser and SRS power histories. These preheat sources are added to integrated hohlraum simulations. To conserve energy and match the measured bang-time, an additional amount of backscattered energy equal to that added for the 18 keV preheat component is removed from the inner laser quads. This is equivalent to saying that the SRS backscatter is actually 150% of that measured, but that a third of this is converted to hot electron preheat. The total amount of energy added to the simulation is thus the same with or without electron preheat. The TPD preheat energy is very small, and is not compensated. The spatial location of the preheat source is specified approximately as the location of the inner beams and is illustrated schematically in Figure 9(b).

Figure 10 shows the relative impact of the electron preheating on the fuel adiabat for the two AS HF shots (a) N150115 and (b) N150416. The temporal histories of the SRS (blue, dashed) and TPD (green, dashed) preheat sources are shown normalized in both Figure 10(a, b) to the individual maxima of the values for the higher power case, N150416. The vertical scale is offset by 1.0 and ranges from 0 to 1 for ease of comparing the relative timing of shock heating vs. electron preheating on the fuel adiabat. The magnitude of both preheat sources (SRS and TPD) in N150115 is approximately 70% of that in N150416 as indicated in Figure 10, and again the TPD source is much smaller in magnitude than the SRS source. The increase in the fuel adiabat with preheat (red) is compared to that without preheat (black). The increase in adiabat is

approximately doubled for the higher power case N150416. Note also that most of the preheating occurs prior to the appearance of the late-time TPD component, which adds very little to the adiabat increase.

Figure 11 quantifies the impact on the DSR of the simulated increase in adiabat due to electron preheating. For N150115, the small increase in adiabat of Figure 10(a) corresponds to a 2% decrease in the simulated DSR, while for N150416 the larger increase in adiabat of Figure 10(b) results in a nearly 10% decrease in DSR, moving the simulations into better agreement with the measured data (the shaded region shows the range of the data including error bars). Agreement between simulation and data is improved for N150416, but not perfect, and suggests that even more preheat (or more likely a different spatial distribution or directionality of the preheat) may be needed to better explain the observations. Neither simulation agrees with the data (N150115 being a bit low and N150416 remaining high), but the important observation is that the impact of electron preheat is much stronger at higher power, in agreement with the trends seen in the data.

The simulations with added electron preheat also show improved agreement with many other performance metrics. Tables II and III summarize the comparison of the simulations with and without preheat with the data. The improved agreement over a range of measurements supports the experimental observations that electron preheat is playing an increased role as laser power increases.

TABLE II. Performance metrics for lower power adiabat-shaped implosion

Performance metric	Simulation, no preheat	Simulation, with preheat	N150115 data
Yield (10^{16})	0.57	0.51	0.30 ± 0.06
YoC	53%	59%	-
Bang time (ns)	18.84	18.78	18.67 ± 0.1
DSR (%)	4.70	4.61	5.04 ± 0.35
Tion (keV)	3.57	3.44	3.98 ± 0.13
HS Pr (GBar)	185	178	177 ± 20
P0 (μm)	29.1	30.4	28.1 ± 1.1
P2/P0 (%)	23.0	-0.6	-3.1 ± 2.4

TABLE III. Performance metrics for higher power adiabat-shaped implosion

Performance metric	Simulation, no preheat	Simulation, with preheat	N150416 data
Yield (10^{16})	1.9	1.6	0.7 ± 0.1
YoC	37%	44%	-
Bang time (ns)	17.64	17.56	17.53 ± 0.02
DSR (%)	5.68	5.23	4.65 ± 0.32
Tion (keV)	5.16	4.89	5.36 ± 0.18
HS Pr (GBar)	334	315	222 ± 23
P0 (μm)	28.1	31.8	28.4 ± 1.2
P2/P0 (%)	27.5	8.3	-6.3 ± 2.0

For both shots, the simulated yield, bang time, DSR, and hot-spot (HS) pressure all show improved agreement with the measured values when electron preheat is added. The simulated ion temperature falls below the data as has been consistently observed in high-foot shots [24]. The hot-spot size, P0, increases with preheat and is slightly larger than the data for both shots. Interestingly, the low-mode P2 distortion comes into significantly better agreement with the data for the simulations including preheat. This is a result of the way the 18 keV preheat component is compensated by an additional backscatter loss on the inner cones, which drives a more pancaked implosion.

VI. SUMMARY AND FUTURE DIRECTIONS

The adiabat-shaping campaign on NIF was performed to controllably assess the relative contributions of ablation-front stability vs. fuel compression on the performance of indirectly-drive capsule implosions. The improvements in performance that have been demonstrated were the result of small changes to the foot of the laser pulse, which made up less than 0.5% of the total laser pulse energy.

With regard to ablation-front stability, it has been shown that a small increase in the energy (+6.8 kJ) of the initial picket pulse produced a substantial reduction in ablation-front instability growth in low-foot implosions as measured by Hydro-Growth Radiography experiments. This

improvement in stability resulted in a substantial increase in neutron yield (3-10X over companion shots from the NIC database) of DT layered implosions with no loss of fuel compression as measured by the neutron Down-Scattered Ratio (DSR). The ablation-front stability was shown to be extremely sensitive to the delivered picket energy, and substantially more reduction in growth is predicted to occur for an additional 10 kJ increase in the picket energy. Such experiments to test the limits and maximize ablation front stability have yet to be performed. In recent years it has become clear, however, that a dominant perturbation source is present in all NIF implosions arising from interactions at the ablation front with the capsule support tent. The current focus of the ICF Program is therefore on developing and demonstrating an improved capsule support method (no tent), which will minimize perturbations and therefore maximize the stability improvement demonstrated by adiabat-shaping.

With regard to fuel compression, it has been shown that a small decrease in the laser trough power (-3 TW) has resulted in a reduction in fuel adiabat in high-foot implosions as quantified in keyhole shock timing measurements. This, in turn, has demonstrated a significant increase in fuel compression (+36%) in layered DT implosions as measured by the DSR. Increased electron preheating at higher laser power, however, appears to offset the gains in fuel compression achieved by adiabat-shaping. This is confirmed by three experimental observations: a decrease in DSR with increasing laser power, a systematic decrease in measured Au isotope ratios, which are proportional to the down-scattered neutron fraction, and measured x-ray hot-spot radii, which show no increase in convergence as peak laser power is increased by 18% from 328 to 388 TW. Integrated hohlraum simulations with a supra-thermal electron preheat model were also performed and confirm this power-dependent preheat degradation on the fuel adiabat, which appears to offset the gains in fuel compression achieved by adiabat-shaping at lower laser power. This power-dependent preheat mechanism is also a likely candidate for explaining the compression limit observed in the high-foot database [24] as well as possibly explaining the lower DSR for higher-power, “coasting” NIC implosions (see Figure 2 of ref. [19]). To take full advantage of the increased fuel compression offered by adiabat-shaping, the ICF Program is current focused on developing improved hohlraum configurations with lower density gas-fills that have demonstrated a substantial reduction in electron preheat [59]. With the development of such a hohlraum environment, the full potential of adiabat-shaping may be realized as the implosions are pushed to higher power.

VII. ACKNOWLEDGEMENTS

This work was performed under the auspices of the Lawrence Livermore National Security, LLC, (LLNS) under Contract DE-AC52-07NA27344. The authors would also like to acknowledge the many insightful conversations on this work with Dov Shvarts and Riccardo Betti.

VIII. REFERENCES

- [1] E. I. Moses, R. Boyd, B. Remington, C. Keane, and R. Al-Ayat, *Phys. Plasmas* **16**, 041006 (2009).
- [2] B. J. Kozioziemski, E. R. Mapoles, J. D. Sater, A. A. Chernov, J. D. Moody, J. B. Lugten, and M. A. Johnson, *Fusion Sci. and Tech.* **59**, 14 (2011).
- [3] J. D. Lindl, P. Amendt, R. L. Berger, S. G. Glendinning, S. H. Glenzer, S. W. Haan, R. L. Kauffman, O. L. Landen, and L. J. Suter, *Phys. Plasmas* **11**, 339 (2004).
- [4] S. W. Haan, J. D. Lindl, D. A. Callahan, D. S. Clark, J. D. Salmonson, B. A. Hammel, L. J. Atherton, R. C. Cook, M. J. Edwards, S. Glenzer, A. V. Hamza, S. P. Hatchett, M. C. Herrmann, D. E. Hinkel, D. D. Ho, H. Huang, O. S. Jones, J. Kline, G. Kyrala, O. L. Landen, B. J. MacGowan, M. M. Marinak, D. D. Meyerhofer, J. L. Milovich, K. A. Moreno, E. I. Moses, D. H. Munro, A. Nikroo, R. E. Olson, K. Peterson, S. M. Pollaine, J. E. Ralph, H. F. Robey, B. K. Spears, P. T. Springer, L. J. Suter, C. A. Thomas, R. P. Town, R. Vesey, S. V. Weber, H. L. Wilkens, and D. C. Wilson, *Phys. Plasmas* **18**, 051001 (2011).
- [5] A. J. MacKinnon, N. B. Meezan, J. S. Ross, S. Le Pape, L. Berzak Hopkins, L. Divol, D. Ho, J. Milovich, A. Pak, J. Ralph, T. Döppner, P. K. Patel, C. Thomas, R. Tommasini, S. Haan, A. G. MacPhee, J. McNaney, J. Caggiano, R. Hatarik, R. Bionta, T. Ma, B. Spears, J. R. Rygg, L. R. Benedetti, R. P. J. Town, D. K. Bradley, E. L. Dewald, D. Fittinghoff, O. S. Jones, H. R. Robey, J. D. Moody, S. Khan, D. A. Callahan, A. Hamza, J. Biener, P. M. Celliers, D. G. Braun, D. J. Erskine, S. T. Prisbrey, R. J. Wallace, B. Kozioziemski, R. Dylla-Spears, J. Sater, G. Collins, E. Storm, W. Hsing, O. Landen, J. L. Atherton, J. D. Lindl, M. J. Edwards, J. A. Frenje, M. Gatu-Johnson, C. K. Li, R. Petrasso, H. Rinderknecht, M. Rosenberg, F. H. S_eguina, A. Zylstra, J. P. Knauer, G. Grim, N. Guler, F. Merrill, R. Olson, G. A. Kyrala, J. D. Kilkenny, A. Nikroo, K. Moreno, D. E. Hoover, C. Wild, and E. Werner, *Phys. Plasmas* **21**, 056318 (2014).
- [6] A. N. Simakov, D. C. Wilson, S. A. Yi, J. L. Kline, D. S. Clark, J. L. Milovich, J. D. Salmonson, and S. H. Batha, *Phys. Plasmas* **21**, 022701 (2014).
- [7] L. Rayleigh, *Proc. London Math. Soc.* **XIV**, 170 (1883).
- [8] G. Taylor, *Proc. R. Soc. London, Ser. A* **201**, 192 (1950).

- [9] R. D. Richtmyer, *Commun. Pure Appl. Math.* **13**, 297 (1960).
- [10] E. E. Meshkov, *Sov. Fluid Dyn.* **4**, 101 (1969).
- [11] V. N. Goncharov *Phys. Rev. Lett.* **82**, 2091(1999).
- [12] N. Metzler, A. L. Velikovich, and J. H. Gardner, *Phys. Plasmas* **6**, 3283 (1999).
- [13] Y. Aglitskiy, A. L. Velikovich, M. Karasik, V. Serlin, C. J. Pawley, A. J. Schmitt, S. P. Obenschain, A. N. Mostovych, J. H. Gardner, and N. Metzler, *Phys. Rev. Lett.* **87**, 265001 (2001).
- [14] Y. Aglitskiy, A. L. Velikovich, M. Karasik, V. Serlin, C. J. Pawley, A. J. Schmitt, S. P. Obenschain, A. N. Mostovych, J. H. Gardner, N. Metzler, *Phys. Plasmas* **9**, 2264 (2002).
- [15] O. V. Gotchev, V. N. Goncharov, J. P. Knauer, T. R. Boehly, T. J.B. Collins, R. Epstein, P. A. Jaanimagi, and D. D. Meyerhofer, *Phys. Rev. Lett.* **96**, 115005 (2006).
- [16] S. Atzeni and J. Meyer-Ter-Vehn, “The Physics of Inertial Fusion”, Clarendon Press, Oxford (2004).
- [17] P. Michel, L. Divol, E. A. Williams, S. Weber, C. A. Thomas, D. A. Callahan, S. W. Haan, J. D. Salmonson, S. Dixit, D. E. Hinkel, M. J. Edwards, B. J. MacGowan, J. D. Lindl, S. H. Glenzer, and L. J. Suter, *Phys. Rev. Lett.* **102**, 025004 (2009).
- [18] G. A. Kyrala, J. L. Kline, S. Dixit, S. Glenzer, D. Kalantar, D. Bradley, N. Izumi, N. Meezan, O. Landen, D. Callahan, S. V. Weber, J. P. Holder, S. Glenn, M. J. Edwards, J. Koch, L. J. Suter, S. W. Haan, R. P. J. Town, P. Michel, O. Jones, S. Langer, J. D. Moody, E. L. Dewald, T. Ma, J. Ralph, A. Hamza, E. Dzenitis, and J. Kilkenny, *Phys. Plasmas* **18**, 056307 (2011).
- [19] M. J. Edwards, P. K. Patel, J. D. Lindl, L. J. Atherton, S. H. Glenzer, S. W. Haan, J. D. Kilkenny, O. L. Landen, E. I. Moses, A. Nikroo, R. Petrasso, T. C. Sangster, P. T. Springer, S. Batha, R. Benedetti, L. Bernstein, R. Betti, D. L. Bleuel, T. R. Boehly, D. K. Bradley, J. A. Caggiano, D. A. Callahan, P. M. Celliers, C. J. Cerjan, K. C. Chen, D. S. Clark, G. W. Collins, E. L. Dewald, L. Divol, S. Dixit, T. Döppner, D. H. Edgell, J. E. Fair, M. Farrell, R. J. Fortner, J. Frenje, M. G. Gatu Johnson, E. Giraldez, V. Yu. Glebov, G. Grim, B. A. Hammel, A. V. Hamza, D. R. Harding, S. P. Hatchett, N. Hein, H. W. Herrmann, D. Hicks, D. E. Hinkel, M. Hoppe, W. W. Hsing, N. Izumi, B. Jacoby, O. S. Jones, D. Kalantar, R. Kauffman, J. L. Kline, J. P. Knauer, J. A. Koch, B. J. Koziemiński, G. Kyrala, K. N. LaFortune, S. Le Pape, R. J. Leeper, R. Lerche, T. Ma, B. J. MacGowan, A. J. MacKinnon,

- A. Macphee, E. R. Mapoles, M. M. Marinak, M. Mauldin, P. W. McKenty, M. Meezan, P. A. Michel, J. Milovich, J. D. Moody, M. Moran, D. H. Munro, C. L. Olson, K. Opachich, A. E. Pak, T. Parham, H.-S. Park, J. E. Ralph, S. P. Regan, B. Remington, H. Rinderknecht, H. F. Robey, M. Rosen, S. Ross, J. D. Salmonson, J. Sater, D. H. Schneider, F. H. Seguin, S. M. Sepke, D. A. Shaughnessy, V. A. Smalyuk, B. K. Spears, C. Stoeckl, W. Stoeffl, L. Suter, C. A. Thomas, R. Tommasini, R. P. Town, S. V. Weber, P. J. Wegner, K. Widman, M. Wilke, D. C. Wilson, C. B. Yeaman, A. Zylstra, *Phys. Plasmas* **20**, 070501 (2013).
- [20] S. P. Regan, R. Epstein, B. A. Hammel, L. J. Suter, H. A. Scott, M. A. Barrios, D. K. Bradley, D. A. Callahan, C. Cerjan, G. W. Collins et al., *Phys. Rev. Lett.* **111**, 045001 (2013).
- [21] T. Ma, S. V. Weber, N. Izumi, P. T. Springer, P. K. Patel, M. H. Key, L. J. Atherton, L. R. Benedetti, D. K. Bradley, D. A. Callahan et al., *Phys. Rev. Lett.* **111**, 085004 (2013).
- [22] H.-S. Park, O. A. Hurricane, D. A. Callahan, D. T. Casey, E. L. Dewald, T. R. Dittrich, T. Döppner, D. E. Hinkel, L. F. B. Hopkins, S. Le Pape *et al.*, *Phys. Rev. Lett.* **112**, 055001 (2014).
- [23] T. R. Dittrich, O. A. Hurricane, D. A. Callahan, E. L. Dewald, T. Döppner, D. E. Hinkel, L. F. Berzak Hopkins, S. Le Pape, T. Ma, J. L. Milovich *et al.*, *Phys. Rev. Lett.* **112**, 055002 (2014).
- [24] O. A. Hurricane, D. A. Callahan, D. T. Casey, P. M. Celliers, C. Cerjan, E. L. Dewald, T. R. Dittrich, T. Döppner, D. E. Hinkel, L. F. Berzak Hopkins *et al.*, *Nature* **506**, 343 (2014).
- [25] J. H. Gardner, S. E. Bodner, and J. P. Dahlburg, *Phys. Fluids B* **3**, 1070 (1991).
- [26] A. L. Velikovich, F. L. Cochran, and J. Davis, *Phys. Rev. Lett.* **77**, 853 (1996).
- [27] S. E. Bodner, D. G. Colombant, J. H. Gardner, R. H. Lehmberg, S. P. Obenschain, L. Phillips, A. J. Schmitt, J. D. Sethian, R. L. McCrory, W. Seka, C. P. Verdon, J. P. Knauer, B. B. Afeyan, H. T. Powell, *Phys. Plasmas* **5**, 1901 (1998).
- [28] K. Anderson and R. Betti, *Phys. Plasmas* **10**, 4448 (2003).
- [29] V. N. Goncharov, J. P. Knauer, P. W. McKenty, P. B. Radha, T. C. Sangster, S. Skupsky, R. Betti, R. L. McCrory, and D. D. Meyerhofer, *Phys. Plasmas* **10**, 1906 (2003).
- [30] R. Betti, K. Anderson, J. Knauer, T. J. B. Collins, R. L. McCrory, P. W. McKenty, and S. Skupsky, *Phys. Plasmas* **12**, 042703 (2005).
- [31] V. A. Smalyuk, V. N. Goncharov, K. S. Anderson, R. Betti, R. S. Craxton, J. A. Delettrez, D. D. Meyerhofer, S. P. Regan, and T. C. Sangster, *Phys. Plasmas* **14**, 032702 (2007).

- [32] J. L. Peterson, L. F. Berzak Hopkins, O. S. Jones, and D. S. Clark, *Phys. Rev E* **91**, 031101 (2015).
- [33] J. L. Peterson, D. S. Clark, L. P. Masse, and L. J. Suter, *Phys. Plasmas* **21**, 092710 (2014).
- [34] D. S. Clark, J. L. Milovich, D. E. Hinkel, J. D. Salmonson, J. L. Peterson, L. F. Berzak Hopkins, D. C. Eder, S. W. Haan, O. S. Jones, M. M. Marinak, H. F. Robey, V. A. Smalyuk, and C. R. Weber, *Phys. Plasmas* **21**, 112705 (2014).
- [35] K. S. Raman, V. A. Smalyuk, D. T. Casey, S. W. Haan, D. E. Hoover, O. A. Hurricane, J. J. Kroll, A. Nikroo, J. L. Peterson, H. F. Robey, A., D. S. Clark, B. A. Hammel, O. L. Landen, M. M. Marinak, D. H. Munro, K. J. Peterson, and J. Salmonson, *Phys. Plasmas* **21**, 072710 (2014).
- [36] V. A. Smalyuk, D. T. Casey, D. S. Clark, M. J. Edwards, S.W. Haan, A. Hamza, D. E. Hoover, W.W. Hsing, O. Hurricane, J. D. Kilkenny, J. Kroll, O. L. Landen, A. Moore, A. Nikroo, L. Peterson, K. Raman, B. A. Remington, H. F. Robey, S. V. Weber, and K. Widmann, *PRL* **112**, 185003 (2014).
- [37] D. T. Casey, V. A. Smalyuk, K. S. Raman, J. L. Peterson, L. Berzak Hopkins, D. A. Callahan, D. S. Clark, E. L. Dewald, T. R. Dittrich, S. W. Haan, D. E. Hinkel, D. Hoover, O. A. Hurricane, J. J. Kroll, O. L. Landen, A. S. Moore, A. Nikroo, H.-S. Park, B. A. Remington, H. F. Robey, J. R. Rygg, J. D. Salmonson, R. Tommasini, and K. Widmann, *Phys. Rev. E* **90**, 011102 (2014).
- [38] J. L. Peterson, D. T. Casey, O. A. Hurricane, K. S. Raman, H. F. Robey, and V. A. Smalyuk, *Phys. Plasmas* **22**, 056309 (2015).
- [39] A. G. MacPhee, J. L. Peterson, D. T. Casey, D. S. Clark, S. W. Haan, O. S. Jones, O. L. Landen, J. L. Milovich, H. F. Robey, and V. A. Smalyuk, *Phys. Plasmas* **22**, 080702 (2015).
- [40] H. F. Robey, T. R. Boehly, P. M. Celliers, J. H. Eggert, D. Hicks, R. F. Smith, R. Collins, M. W. Bowers, K. G. Krauter, P. S. Datte, D. H. Munro, J. L. Milovich, O. S. Jones, P. A. Michel, C. A. Thomas, R. E. Olson, S. Pollaine, R. P. J. Town, S. Haan, D. Callahan, D. Clark, J. Edwards, J. L. Kline, S. Dixit, M. B. Schneider, E. L. Dewald, K. Widmann, J. D. Moody, T. Döppner, H. B. Radousky, A. Throop, D. Kalantar, P. DiNicola, A. Nikroo, J. J. Kroll, A. V. Hamza, J. B. Horner, S. D. Bhandarkar, E. Dzenitis, E. Alger, E. Giraldez, C. Castro, K. Moreno, C. Haynam, K. N. LaFortune, C. Widmayer, M. Shaw, K. Jancaitis, T.

- Parham, D. M. Holunga, C. F. Walters, B. Haid, E. R. Mapoles, J. Sater, C. R. Gibson, T. Malsbury, J. Fair, D. Trummer, K. R. Coffee, B. Burr, L. V. Berzins, C. Choate, S. J. Brereton, S. Azevedo, H. Chandrasekaran, D. C. Eder, N. D. Masters, A. C. Fisher, P. A. Sterne, B. K. Young, O. L. Landen, B. M. Van Wonterghem, B. J. MacGowan, J. Atherton, J. D. Lindl, D. D. Meyerhofer, E. Moses, *Phys. Plasmas* **19**, 042706 (2012).
- [41] H. F. Robey, P. M. Celliers, J. L. Kline, A. J. Mackinnon, T. R. Boehly, O. L. Landen, J. H. Eggert, D. Hicks, S. Le Pape, D. R. Farley, M. W. Bowers, K. G. Krauter, D. H. Munro, O. S. Jones, J. L. Milovich, D. Clark, B. K. Spears, R. P. J. Town, S. W. Haan, S. Dixit, M. B. Schneider, E. L. Dewald, K. Widmann, J. D. Moody, T. Döppner, H. B. Radousky, A. Nikroo, J. J. Kroll, A. V. Hamza, J. B. Horner, S. D. Bhandarkar, E. Dzenitis, E. Alger, E. Giraldez, C. Castro, K. Moreno, C. Haynam, K. N. LaFortune, C. Widmayer, M. Shaw, K. Jancaitis, T. Parham, D. M. Holunga, C. F. Walters, B. Haid, T. Malsbury, D. Trummer, K. R. Coffee, B. Burr, L. V. Berzins, C. Choate, S. J. Brereton, S. Azevedo, H. Chandrasekaran, B. K. Young, M. J. Edwards, B. M. Van Wonterghem, B. J. MacGowan, J. Atherton, J. D. Lindl, D. D. Meyerhofer, E. Moses, *Phys. Rev. Lett.* **108**, 215004 (2012).
- [42] D. G. Hicks, B. K. Spears, D. G. Braun, R. E. Olson, C. M. Sorce, P. M. Celliers, G. W. Collins, and O. L. Landen, *Phys. Plasmas* **17**, 102703 (2010).
- [43] K. L. Baker, H. F. Robey, J. L. Milovich, O. S. Jones, V. A. Smalyuk, D. T. Casey, A. G. MacPhee, A. Pak, P. M. Celliers, D. S. Clark, O. L. Landen, J. L. Peterson, L. F. Berzak-Hopkins, C. R. Weber, S. W. Haan, T. D. Döppner, S. Dixit, E. Giraldez, A. V. Hamza, K. S. Jancaitis, J. J. Kroll, K. N. LaFortune, B. J. MacGowan, J. D. Moody, A. Nikroo, and C. C. Widmayer, *et al.*, *Phys. Plasmas* **22**, 052702 (2015).
- [44] L. M. Barker and R. E. Hollenbach, *J. Appl. Phys.* **43**, 4669 (1972).
- [45] P. M. Celliers, D. K. Bradley, G. W. Collins, D. G. Hicks, T. R. Boehly, W. J. Armstrong, *Rev. Sci. Instrum.* **75**, 4916 (2004).
- [46] M. M. Marinak, G. D. Kerbel, N. A. Gentile, O. Jones, D. Munro, S. Pollaine, T. R. Dittrich, and S. W. Haan, *Phys. Plasmas* **8**, 2275 (2001).
- [47] R. P. Drake, “High-Energy-Density Physics”, Springer (2006).
- [48] J. R. Rygg, O. S. Jones, J. E. Field, M. A. Barrios, L. R. Benedetti, G. W. Collins, D. C. Eder, M. J. Edwards, J. L. Kline, J. J. Kroll, O. L. Landen, T. Ma, A. Pak, J. L. Peterson, K. Raman, R. P. J. Town and D. K. Bradley, *Phys. Rev. Lett.* **112**, 195001 (2014).

- [49] S. R. Nagel, S. W. Haan, J. R. Rygg, M. Barrios, L. R. Benedetti, D. K. Bradley, J. E. Field, B. A. Hammel, N. Izumi, O. S. Jones, S. F. Khan, T. Ma, A. E. Pak, R. Tommasini, and R. P. J. Town, *Phys. Plasmas* **22**, 022704 (2015).
- [50] R. Tommasini, J. E. Field, B. A. Hammel, O. L. Landen, S. W. Haan, C. Aracne-Ruddle, L. R. Benedetti, D. K. Bradley, D. A. Callahan, E. L. Dewald, T. Döppner, M. J. Edwards, O. A. Hurricane, N. Izumi, O. A. Jones, T. Ma, N. B. Meezan, S. R. Nagel, J. R. Rygg, K. S. Seagraves, M. Stadermann, R. J. Strauser, and R. P. J. Town, *Phys. Plasmas* **22**, 056315 (2015).
- [51] Milovich *et al.*, to appear in *Phys. Plasmas* (2015).
- [52] D. T. Casey, J. L. Milovich, V. A. Smalyuk, D. S. Clark, H. F. Robey, A. Pak, A. G. MacPhee, K. L. Baker, C. R. Weber, T. Ma, H.-S. Park, T. Döppner, D. A. Callahan, S.W. Haan, P. K. Patel, J. L. Peterson, D. Hoover, A. Nikroo, C. B. Yeamans, F. E. Merrill, P. L. Volegov, D. N. Fittinghoff, G. P. Grim, M. J. Edwards, O. L. Landen, K. N. Lafortune, B. J. MacGowan, C. C. Widmayer, D. B. Sayre, R. Hatarik, E. J. Bond, S. R. Nagel, L. R. Benedetti, N. Izumi, S. Khan, B. Bachmann, B. K. Spears, C. J. Cerjan, M. Gatu Johnson, and J. A. Frenje, *Phys. Rev. Lett.* **115**, 105001 (2015).
- [53] V. A. Smalyuk, H. F. Robey, T. Döppner, O. S. Jones, J. L. Milovich, B. Bachmann, K. L. Baker, L. F. Berzak Hopkins, E. Bond, D. A. Callahan, D. T. Casey, P. M. Celliers, C. Cerjan, D. S. Clark, S. N. Dixit, M. J. Edwards, E. Giraldez, S. W. Haan, A. V. Hamza, M. Hohenberger, D. Hoover, O. A. Hurricane, K. S. Jancaitis, J. J. Kroll, K. N. Lafortune, O. L. Landen, B. J. MacGowan, A. G. MacPhee, A. Nikroo, A. Pak, P. K. Patel, J. L. Peterson, C. R. Weber, C. C. Widmayer, C. Yeamans, *Phys. Plasmas* **22**, 080703 (2015).
- [54] D. A. Shaughnessy, K. J. Moody, N. Gharibyan, P. M. Grant, J. M. Gostic, P. C. Torretto, P. T. Woody, B. B. Bandong, J. D. Despotopoulos, C. J. Cerjan, C. A. Hagmann, J. A. Caggiano, C. B. Yeamans, L. A. Bernstein, D. H. G. Schneider, E. A. Henry, and R. J. Fortner, *Rev. Sci. Instrum.* **85**, 063508 (2014).
- [55] Döppner *et al.*, in preparation for submission to *J. Instrum.* (2015).
- [56] G. P. Schurtz, Ph. D. Nicolai, and M. Busquet, *Phys. Plasmas* **7**, 4238 (2000).
- [57] H. A. Bethe and J. A. Ashkin, *Experimental Nuclear Physics*, (Thomas Wiley, New York, 1956).

- [58] R. M. More, *Atomic Physics in Inertial Confinement Fusion*, Part I, Lawrence Livermore National Laboratory, Livermore, CA, UCRL-84991 (1981); R. M. More, D. Bailey, and Y. T. Lee, *Charge States and Dynamic Screening of Swift Ions*, Oak Ridge National Laboratory, Oak Ridge, Tenn., ORNL Report CONF-82013, p. 155. (1982).
- [59] D. E. Hinkel, Bulletin of the 57th Meeting of the APS Division of Plasma Physics, Savannah, GA (2015).

IX. FIGURE CAPTIONS

- Figure 1. Plot of measured neutron yield vs. DSR. Low-foot shots are shown in blue, high-foot shots in green, and adiabat-shaped shots in magenta.
- Figure 2. (a) Laser power histories for the five shots considered in this study. The standard low-foot (black) and high-foot (red) pulses are shown with dashed lines. The adiabat-shaped versions of the low-foot (blue) and high-foot (green, orange) are shown with solid lines. (b) Measured VISAR shock velocity histories for all four pulses with the same colors as the laser pulses of (a).
- Figure 3. (a) Plot of pressure of the first shock as it traverses the ablator and fuel for all five pulses. Pressure is obtained from simulations precisely tuned to match the measured VISAR data. Adiabat-shaped pulses achieve a high pressure at the ablation front ($r \sim 1100 \mu\text{m}$) and a low pressure in the DT fuel. (b) Plot of fuel adiabat time history for all five pulses. The symbols indicate the adiabat at the time of peak fuel velocity.
- Figure 4. (a) Plot of simulated ablation-front growth factor amplitude (amplitude ratio from $t = 0$ to the time of peak fuel velocity) for all four pulses. (b) Schematic of the Hydro-Growth Radiography (HGR) experimental platform. (c) Measured optical depth growth factor dispersion curves for all four pulses.
- Figure 5. (a) Measured neutron yield vs. DSR for AS LF shot N141123. Companion (non-adiabat-shaped) low-foot shots with nearly identical conditions are shown with blue circles. High-foot shot N150610, with similar laser power and energy, is shown with the green circle. (b) Simulated ablation-front growth factor amplitude dispersion curves comparing the standard low-foot pulse (red), the adiabat-shaped LF pulse as delivered on shot N141123 (black), the requested adiabat-shaped LF pulse (blue), and an adiabat-shaped LF pulse with picket energy increased to 30

kJ (green). The circle symbols show the predicted growth for each of these pulses at the dominant mode number characterizing the localized feature resulting from the capsule support tent.

Figure 6. (a) Plot of laser pulses comparing a lower-power HF pulse (N150610, green, dashed) with the lower-power AS HF pulse (N150115, magenta, dashed), and a higher-power HF pulse (N140520, green, solid) with the higher-power AS HF pulse (N150416, magenta, solid). (b) Plot of measured neutron yield vs. DSR for AS HF shots N150115 and N150416. Companion standard HF shots N150610 and N140520 are shown with the green circles.

Figure 7. (a) Plot of ratio of $^{198}\text{Au}/^{196}\text{Au}$ measured by the Solid Radio-Chemistry (SRC) collection diagnostic vs. DSR. This ratio is proportional to the fuel compression. Adiabatic-shaped and companion HF shots are highlighted. (b) Plot of measured x-ray hot-spot size comparing AS HF shots (N150115, N150416) vs. their companion standard HF shots. The measured hot-spot radii are essentially the same for both adiabatic-shaped shots, despite the increase in laser power.

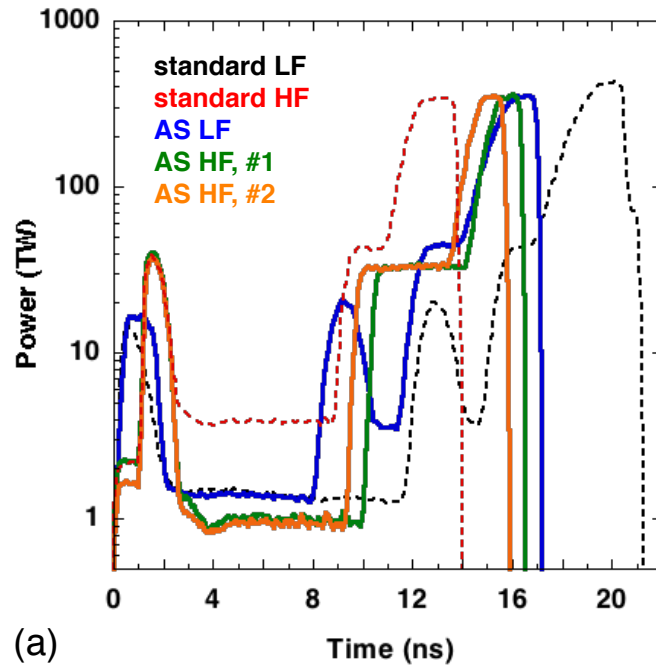
Figure 8. (a) Images of hard x-ray emission from the eHXI diagnostic for AS HF shots (N150115, N150416). (b) Vertical lineouts of emission from eHXI channel 1 (50 keV) for each shot showing $\sim 2X$ increase in emission for the higher power shot N150416.

Figure 9. (a) Plot of measured laser power, SRS back-scattered power, and FFLEX-measured two plasmon decay (TPD, $\times 100$) power histories for adiabatic-shaped shots N150115 (blue) and N150416 (red). (b) Schematic illustration of the computational geometry indicating the location of the hot electron source in the simulations.

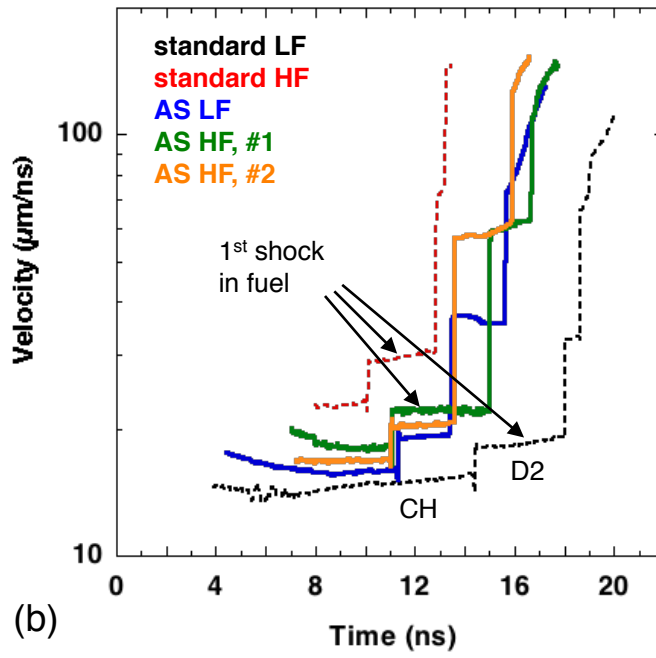
Figure 10. Plot of simulated fuel adiabat without (black) and with electron preheat (red) for (a) lower peak power AS HF shot N150115 and (b) higher power AS HF shot

N150416. The normalized power history of the SRS (blue, dashed) and TPD (green, dashed) electron preheat sources are shown with power normalized to the SRS and TPD maxima of N150416.

Figure 11. Plot of simulated (symbols) vs. measured DSR (gray bands) for (a) N150115 and (b) N150416. Decrease in simulated DSR with the addition of electron preheat is $\sim 5X$ greater for the higher-power adiabat-shaped shot N150416 than for the lower-power shot N150115.

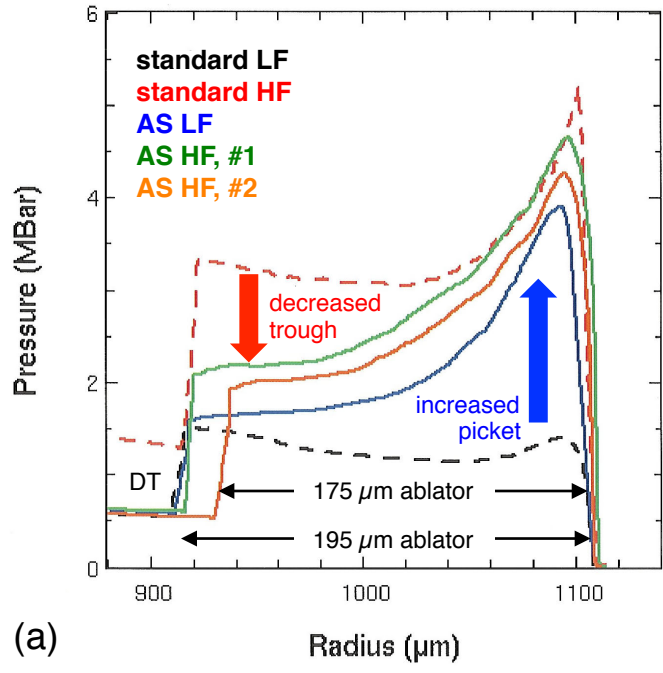


(a)

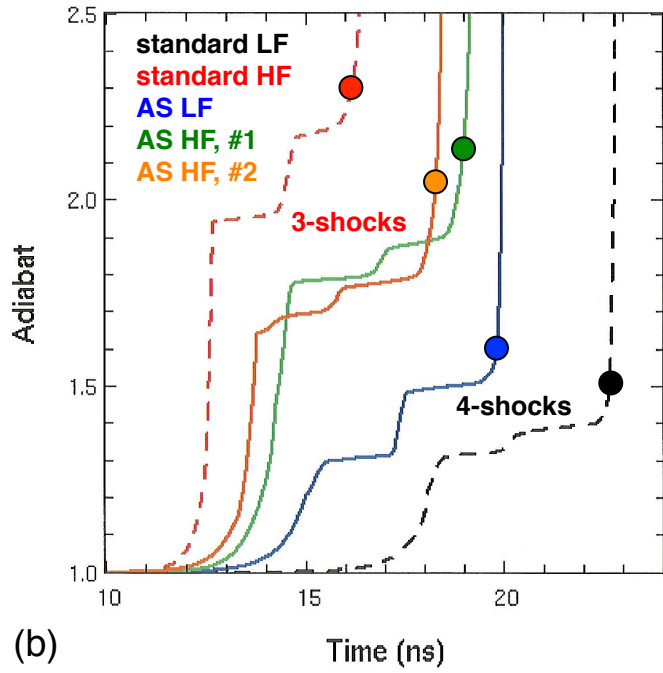


(b)

Figure 2



(a)



(b)

Figure 3

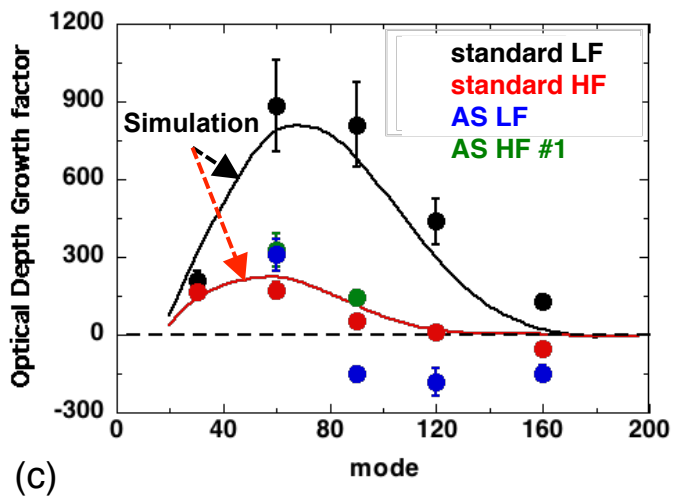
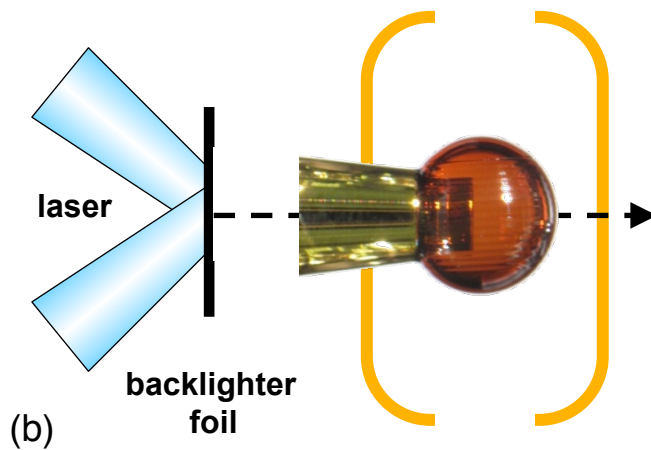
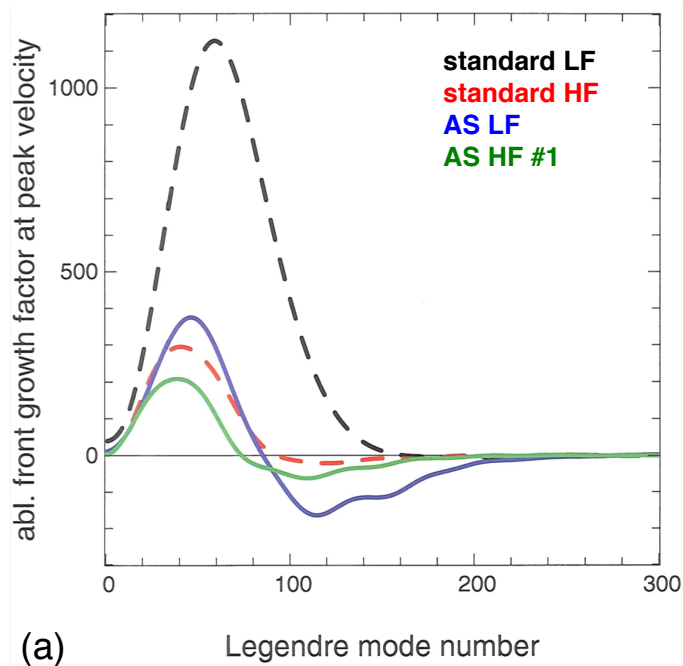


Figure 4

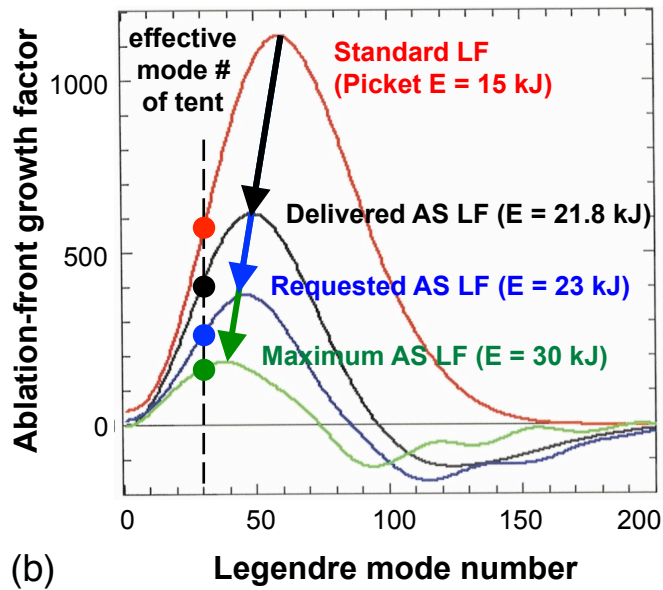
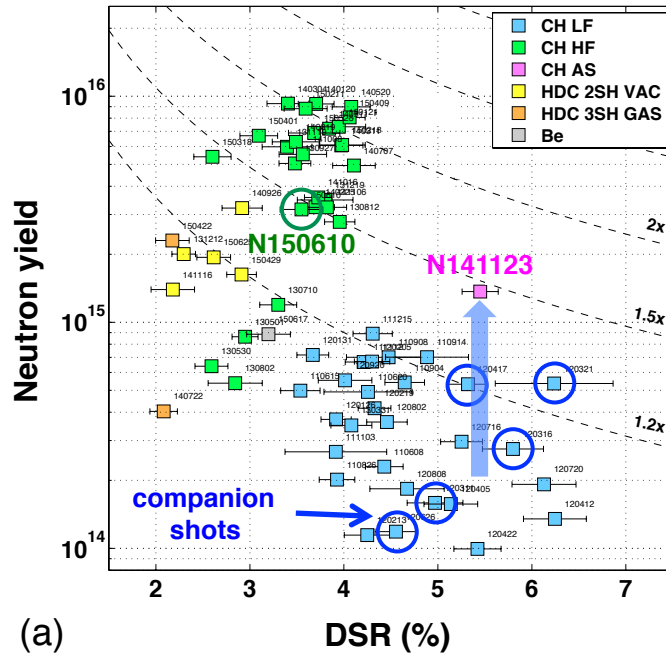


Figure 5

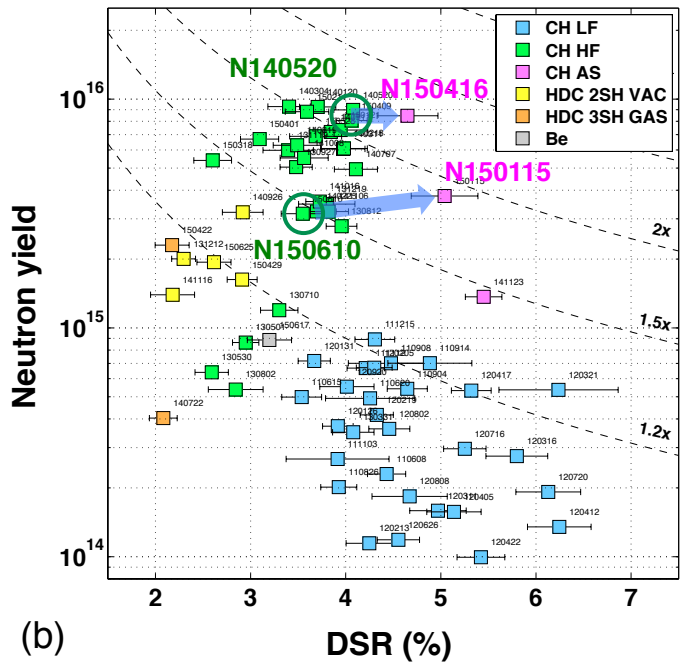
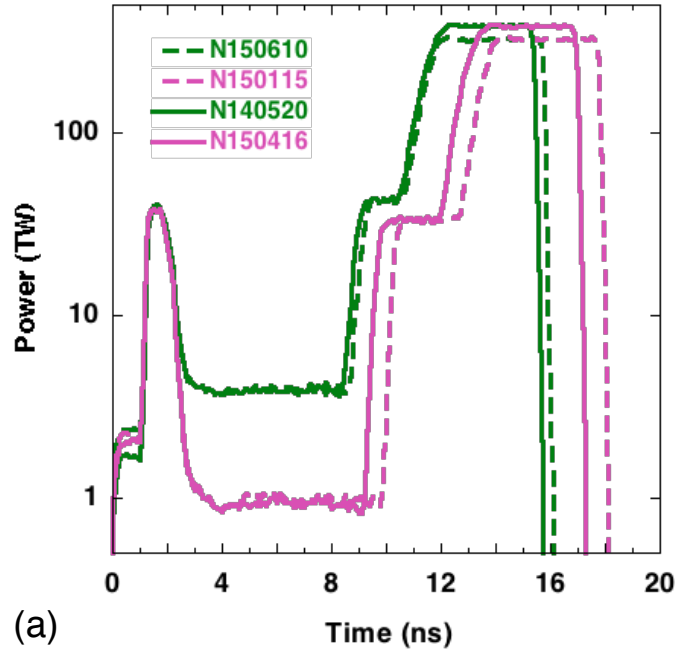


Figure 6

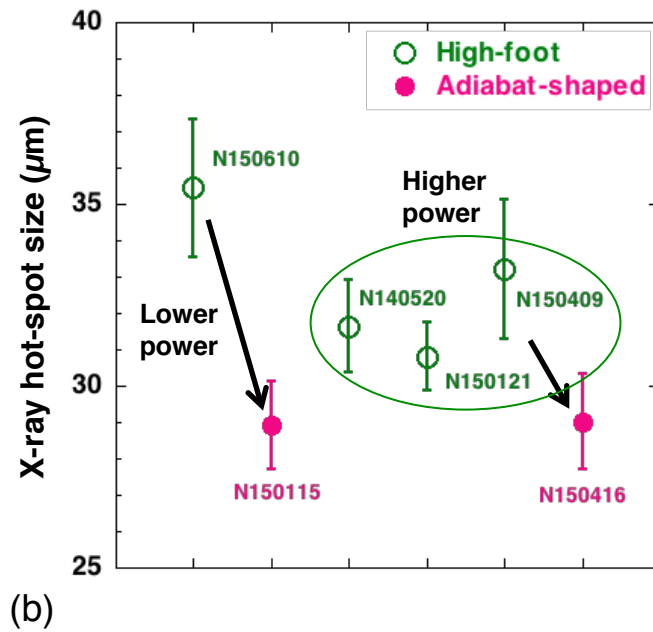
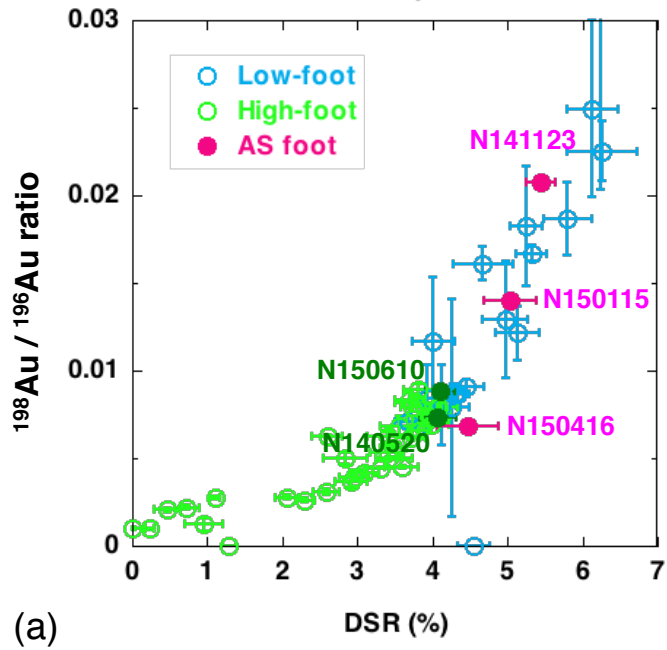


Figure 7

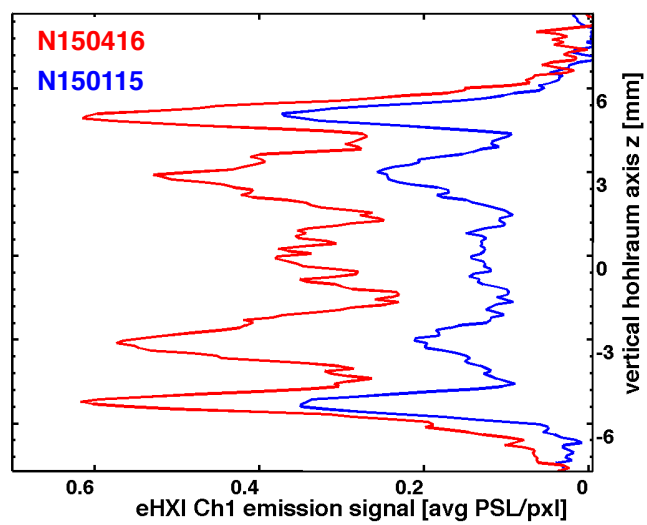
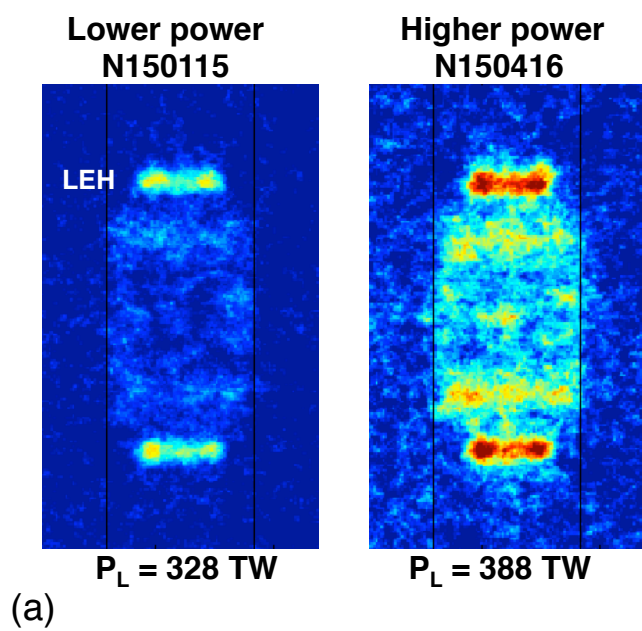


Figure 8

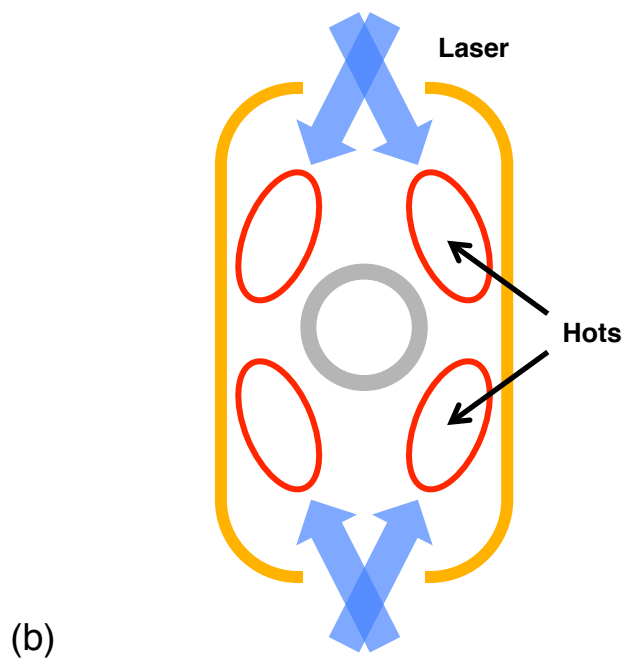
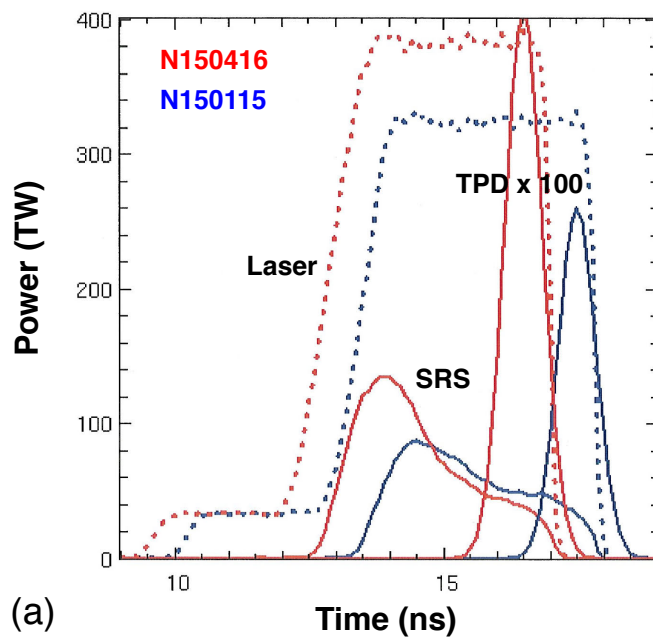
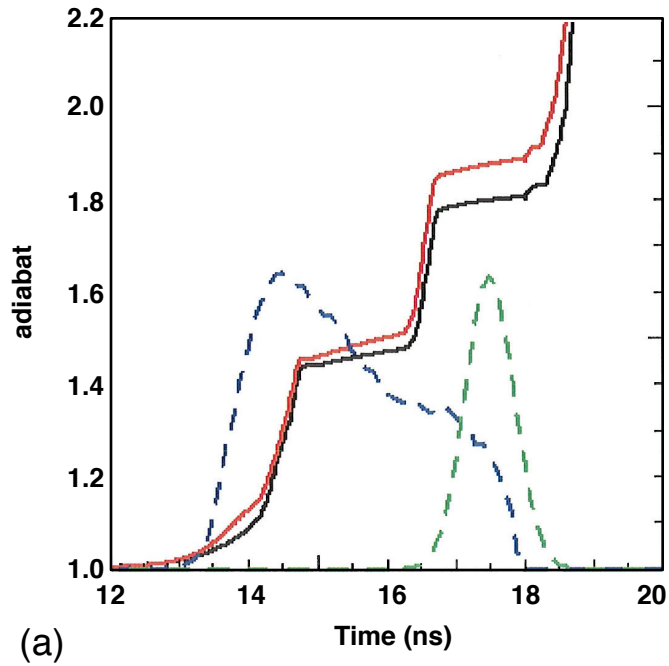
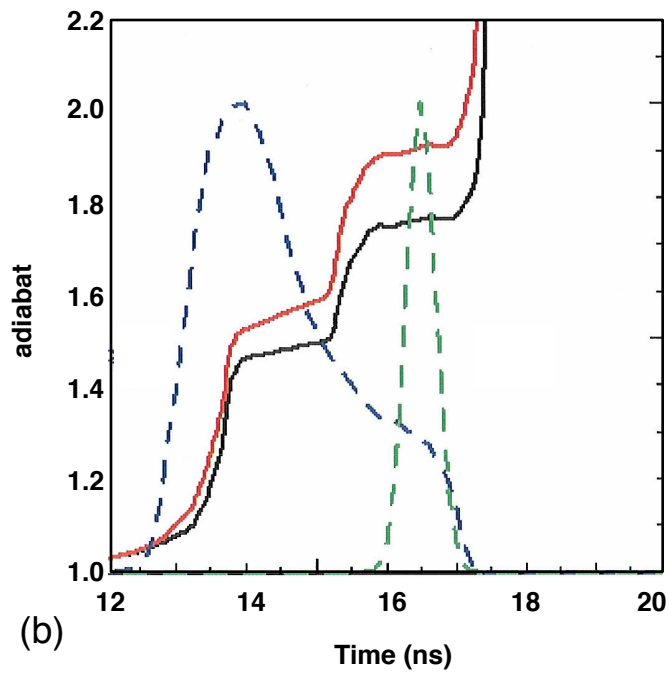


Figure 9



(a)



(b)

Figure 10

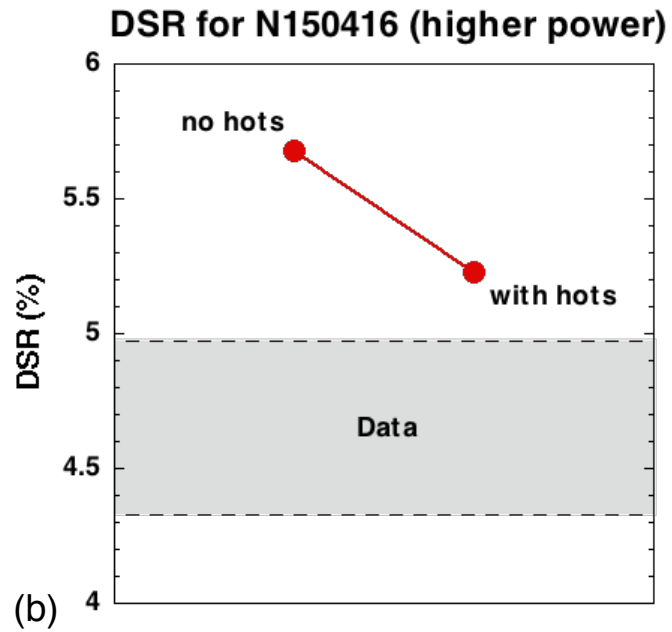
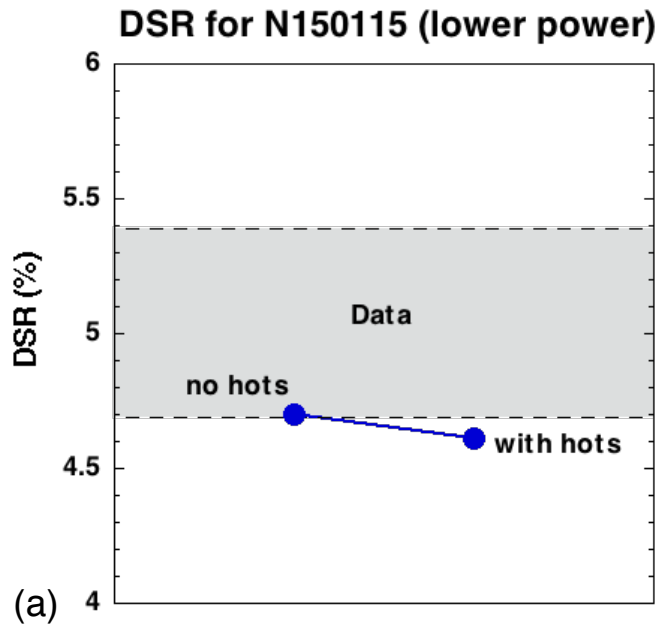


Figure 11